Progress In Electromagnetics Research C, Vol. 116, 157–169, 2021

17–30 GHz Reliable and Compact Analog Phase Shifter Using Lateral Micromachined SP7T Switches, and DMTL Arrays

Sukomal Dey[1, *], Shiban K. Koul[2], Ajay K. Poddar[3], and Ulrich Rohde[3]

Abstract—In this work, a radio frequency (RF) micro-electromechanical system (MEMS) based analog phase shifter is presented over 17–30 GHz. The proposed phase shifter is made using two back-to-back single-pole-seven-throw (SP7T) switches and connected through seven distributed MEMS transmission lines (DMTL). The SP7T switch is designed with lateral electrostatic actuation and demonstrates measured average return loss of > 11.3 dB, insertion loss of < 5.94 dB, and isolation of > 22 dB up to 30 GHz. Total area of the SP7T switch is only 0.89 mm^2 including bias lines and pads. The proposed wide-band phase shifter can be tuned at all the frequencies between 17 and 30 GHz. Phase shifter gives measured average insertion loss of < 6.94 dB, return loss of > 10 dB, and phase error of $\sim 1^\circ$ at 17 GHz to 30 GHz over 500 MHz bandwidth. All phase shifts can be tracked with a resolution of 22.5° based on predefined actuation voltages. Total area of the fabricated device is ~ 11.72 mm^2. In addition, switches and phase shifter work satisfactorily > 1 billion cycles with 0.1–1 W of RF power. The proposed phase shifter bank gives phase shifting performances at each frequency over 17–30 GHz with a constant resolution utilizing analog tuning, and it operates > 1 billion cycles of reliability with 1 W of RF power.

1. INTRODUCTION

Broadband phase shifter is one of the essential radio frequency (RF) components for next generation wideband or multi-band systems. One wideband phase shifter can replace many phase shifters within a system and reduce the system complexity to a reasonable extent [1]. Different kinds of technology have been adopted so far for microwave phase shifter, including CMOS, low temperature co-fired ceramic (LTCC), ferroelectric, photonic, liquid-crystal and radio frequency microelectromechanical system (RF MEMS) [2–4]. Out of them, RF MEMS is one of the non-slid state technologies and demonstrates low loss, high linearity, low power consumption, excellent group delay, and low phase error [5].

Different types of phase shifters have been reported in the literature over last two decades [6–23] in narrowband or wideband. One of the major challenges of a wideband phase shifter is to track any frequency over a wide spectrum without compromising other performances like loss, matching, and phase error. In addition, all these reported phase shifters are unable to generate any phase shift over broadband. This work primarily focuses on all these aspects to a reasonable limit over 17–30 GHz using micromachining technology. The proposed phase shifter has the capability to provide phase shift based on analog tuning with 22.5° steps at each frequency over 17–30 GHz. Nevertheless, phase shifter can cover the range of 0°–337.5° with $< 1^\circ$ of phase error. The main control elements on the proposed device are single-pole-seven-throw (SP7T) switches and MEMS bridges. The switching action of this work was reported in [24, 26] where prime focus was given on the design and development of the SP7T switches over 1–30 GHz. In addition, complete fabrication details of this work can be found in [24].

Received 20 August 2021, Accepted 17 October 2021, Scheduled 29 October 2021

* Corresponding author: Sukomal Dey (sukomal28@gmail.com).

[1] Department of Electrical Engineering, Indian Institute of Technology, Palakkad, India. [2] Centre for Applied Research in Electronics, Indian Institute of Technology, Delhi, India. [3] Synergy Microwave Corporation, NJ, USA.

The present work focuses on the wideband phase shifter utilizing the same SP7T switch with more additional experimental data in the subsequent sections.

The work is divided into four phases. Phase I briefly discusses the proposed design topology of the wide-band phase shifter. Phase II focuses on the detailed experimental analysis of the MEMS switches. Phase III describes performance characterization of the proposed phase shifter. Phase IV provides extensive experimental analysis on the devices power handling and reliability up to 1 billion (B) actuation cycles. Finally, results are compared with the present state-of-the-art performances.

2. PROPOSED DESIGN TOPOLOGY OF THE WIDEBAND PHASE SHIFTER: PHASE I

In this work, a wideband phase shifter is designed using a simple topology, as shown in Fig. 1. A microfabricated image of the SP7T switch is also depicted in Fig. 1. In this topology, seven DMTLs are connected between two lateral SP7T switches. All DMTL cells have different dimensions in terms of length, and they are loaded with fifteen MEMS bridges with an airgap of 2.5 µm. The proposed topology is inspired from the switched line-based phase shifters, but here each line acts as a phase shifter. Conventional 2-bit and 4-bit phase shifters were proposed with two and four SP4T switches in [20, 21, 25]. Later, two SP16T switches were used for a 4-bit phase shifter [26]. The present technique needs two SP7T switches for an analog type phase shifter operation followed by seven DMTLs. Nevertheless, all these above-mentioned phase shifters work over narrow frequency band [20, 21, 24, 25], but the reported structure can provide a wideband operation with flexible phase steps followed by controlled and predefined electrostatic actuations.

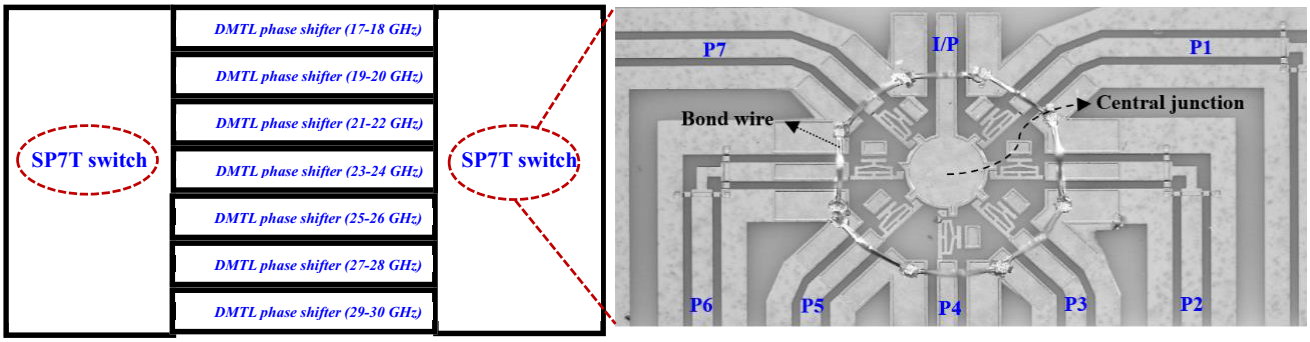

Figure 1. Schematic of the proposed wideband phase shifter array using two MEMS SP7T switches and seven DMTL structures. Inset shows microfabricated image of the single-pole-seven-throw (SP7T) switch [24].

3. DESIGN AND MEASUREMENTS OF THE LATERAL MEMS SWITCHES: PHASE II

The microscopic image of the lateral MEMS switches is depicted in Fig. 2(a) [26]. Initially, single MEMS switch was fabricated, and later the same switch was used to develop SP7T configuration. The performances of the single switch were extensively measured to ensure the optimum switch behaviours. The switch was implemented on a 50 Ω coplanar waveguide (CPW) transmission line ($G = 35$ µm, $W = 80$ µm) on an alumina substrate ($\varepsilon_r = 9.8$) with a gold of thickness 2 µm. The switch is placed on the center CPW line. Complete design details of the single switch and its complete performance analysis are presented in [26]. Fig. 2(b) shows the equivalent circuit of the lateral MEMS series switch. Fig. 3(a) shows switch R_c variation from 1.85–1.73 Ω with 90–103 V of bias voltage. Finally, 95 V was chosen from it for stable operation with proper contact. Measured switching time of 38 µsec [see Fig. 3(b)] and mechanical resonance frequency of 0.28 MHz were obtained from the switch [26], respectively. Finally, S-parameter performances of the single switch are tested up to 30 GHz using Agilent Vector Network

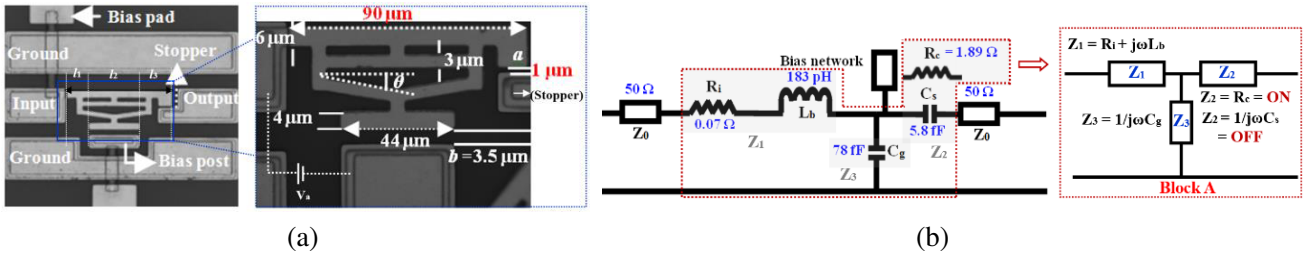

(a) (b)

Figure 2. (a) Fabricated microscopic image of the single lateral MEMS switch, all structural parameters are marked and (b) its equivalent circuit model [26].

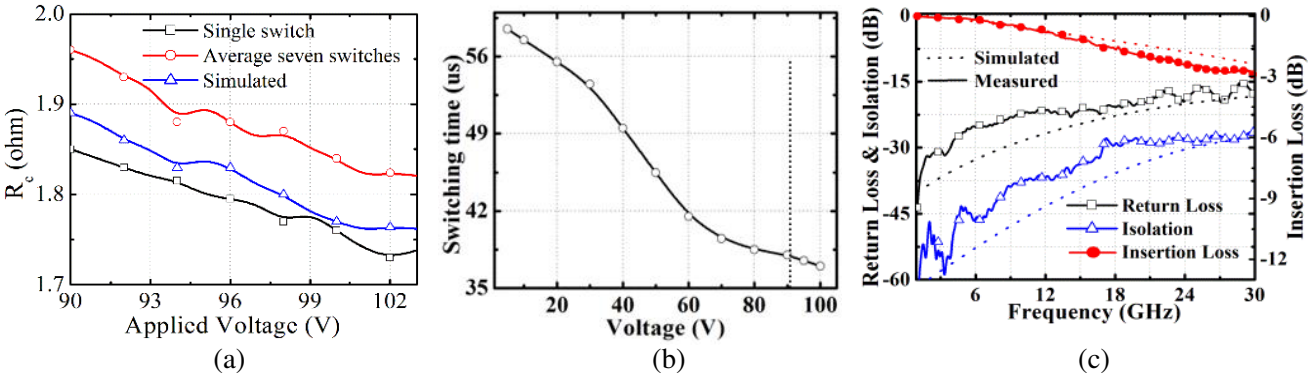

(a) (b) (c)

Figure 3. Measured (a) contact resistance versus applied voltage, (b) switching time, and (c) S-parameter performances of the single MEMS switch.

Analyzer (E8361C) with cascade dc probes and calibrated using short-open-load-thru (SOLT) standards to the probe tips. Switch demonstrates measured return loss of better than 12 dB with worst case insertion loss of $\sim$ 3 dB and isolation of better than 28 dB up to 30 GHz, as shown in Fig. 3(c). The individual circuit parameters were obtained from the measured S-parameter data using equations given in [26] and compared with the measured results. Results show good agreement between simulated and measured responses. In addition, all extracted parameters are mentioned in Fig. 2(b) for clarity.

After successful completion of design and measurement phases of the single switch, SP7T switch was developed with seven identical switches anchored with a 45° angle between one another. Microscopic image of the SP7T switch is depicted in Fig. 1. The total area of SP7T switches is 0.89 mm^2 including bias lines and pads. Moreover, CPW ground lines are connected with bond wires in order to remove CPW odd-modes during the operation. Each switch carries a dedicated bias pad and actuated. Each switch was actuated at a time, and cantilever beam was connected with the respective output transmission line. Note that input line of the switch is connected with a central junction where all seven switches get RF connection. Hence, central junction plays a crucial role in the design, and radius of this junction was extensively optimized in full wave simulator. Note that central junction has a role on the overall matching (S_{11}) to the structure. Needless to say, a similar actuation mechanism ($a \ll b$) was adopted throughout over the same bias voltage [see Fig. 2(a)]. The SP7T switch gives measured return loss of better than 11.3 dB, worst case insertion loss of 5.94 dB, and isolation better than 22 dB up to 30 GHz [26]. All measured responses are validated using circuit model and can be found in [26].

4. DESIGN AND TESTING OF THE WIDEBAND MEMS PHASE SHIFTER: PHASE III

DMTL based technique is used in this work to design seven analog phase shifters. A high impedance ($> 50\,\Omega$) CPW line was loaded with MEMS bridges with periodic spacing. MEMS bridges are connected

with the CPW grounds, and they act as a varactors based on the electrostatic actuation. It adds distributed capacitances along the length of the line. The capacitance variation changes the phase velocity and produces a differential phase shift. This phase shift is the impedance difference between non-actuated and actuated states.

The primary aim of any phase shifter design is to achieve required phase shift with minimum loss and good matching (< 10 dB) over the band of interest. Note that seven different analog DMTL phase shifters were designed, fabricated, and tested separately to ensure optimum device performance. Each phase shifter works at two frequencies based on the electrostatic actuation. It starts from the 17–18 GHz and ends at 29–30 GHz. The quality of the MEMS bridge was checked experimentally, and the design was inspired from [28]. Complete design details of the single MEMS bridge can be found in [27, 28]. The microscopic image of the fabricated unit cell phase shifter and its equivalent circuit model are shown in Figs. 4(a)–(b), respectively. Measured RF capacitance variation of the bridge shows pull in at 92 V [see Fig. 4(c)]. Measured RF capacitances variations are given at the lowest (17 GHz) and highest (30 GHz) frequencies. The region of phase shifter operation is marked in Fig. 4(c), and it shows that the entire phase shifter operates between 66 and 80 V actuation voltages (V_b) from 17 to 30 GHz. The S-parameter performances of the unit cell were critically observed at V_b of 66 V and 88 V, as depicted in Fig. 4(d). Results show measured return loss of > 14 dB and insertion loss of < 1.1 dB between 17 and 30 GHz. Please note that measured phase shift of $\sim 22.5°$ was achieved between 80 and 66 V bias voltages over 17 GHz to 30 GHz frequency ranges. Note that all bridges operate within a point of stability (maximum V_b of 80 V, Pull-in = 92 V). It gives a high degree of stability over a long range of operation.

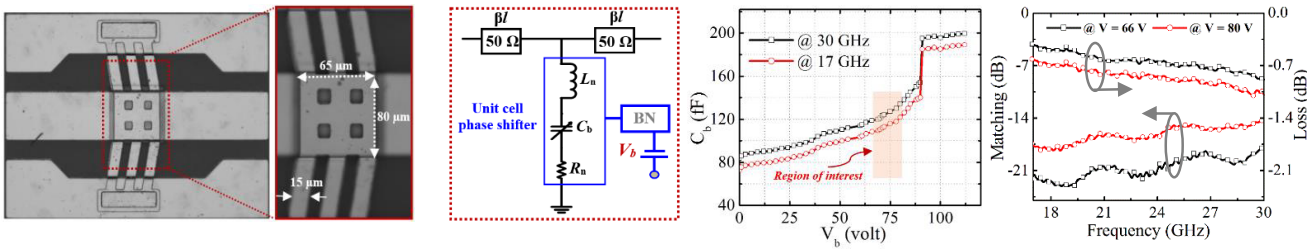

(a) (b) (c) (d)

Figure 4. (a) Fabricated image, (b) equivalent circuit model, (c) measured changes in MEMS bridge capacitance (C_b) with V_b values, and (d) measured S-parameter performances at 66 V and 80 V of V_b of the unit cell.

Finally, fifteen similar MEMS bridges were used to develop a complete phase shifter. All DMTL phase shifter functional parameters like impedances at non-actuated (Z_{lu}) and actuated (Z_{ld}) states, distance between two periodic cells (s)) were optimized in full-wave simulators using Equations (1)–(2) [1]

$$Z_{lu} = \sqrt{\frac{sL_t}{sC_t + C_{lu}}}\,\Omega \quad Z_{ld} = \sqrt{\frac{sL_t}{sC_t + C_{ld}}}\,\Omega \tag{1}$$

$$s = \frac{Z_{ld}c}{\pi f_B Z_0 \sqrt{\varepsilon_{r,eff}}} \tag{2}$$

where C_{lu} and C_{ld} are the loaded up (at Z_{lu}) and actuated state capacitances (at Z_{ld}); sL_t and sC_t are the per unit line inductance and capacitance; Z_0 is the characteristic impedance; $\varepsilon_{r,eff}$ is the effective permittivity; and c is the free space velocity. The Bragg frequency of the structure is 2.5 times of the lowest operating frequency. Differential phase shift ($\Delta\phi$) can be stated as [1];

$$\Delta\phi = \frac{s\omega Z_0 \sqrt{\varepsilon_{r,eff}}}{c}\left(\frac{1}{Z_{lu}} - \frac{1}{Z_{ld}}\right) \text{ rad/sec} \tag{3}$$

Individual phase shifter cells demonstrated maximum average matching and insertion loss of 12 dB and 5.6 dB over 17–30 GHz. Maximum phase error ($\Delta\phi_E$) of $\sim 0.4°$ was obtained at each operating frequency. $\Delta\phi$ were obtained with 66–80 V over the band.

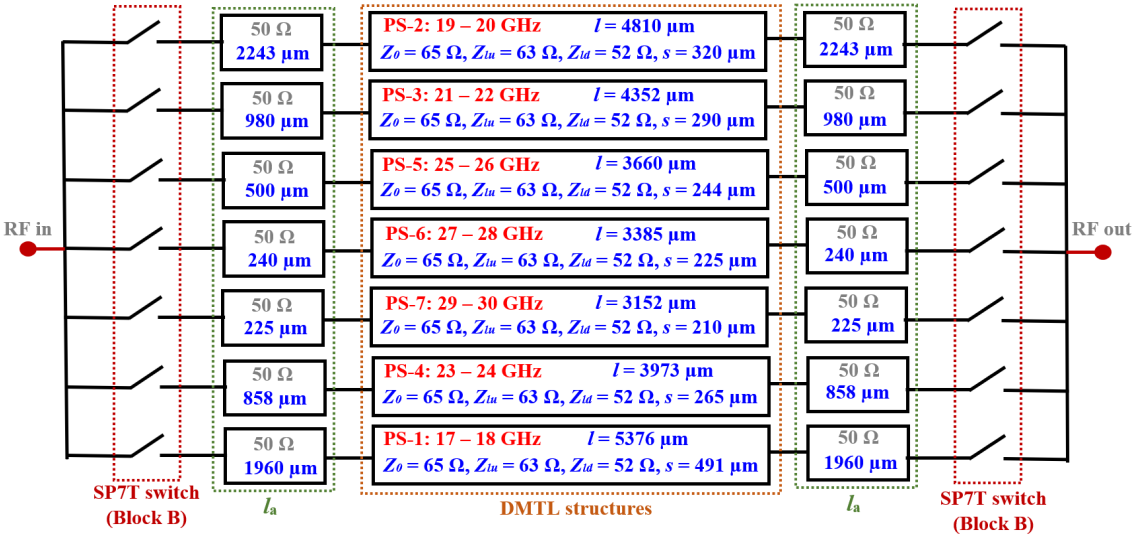

where, Z_0 = unloaded impedance, Z_{lu} = loaded impedance (at $V_b = 0$V), Z_{ld} = loaded impedance (at $V_b = +$V), s = unit cell length, l = DMTL length, and l_a = additional line length.

(a)

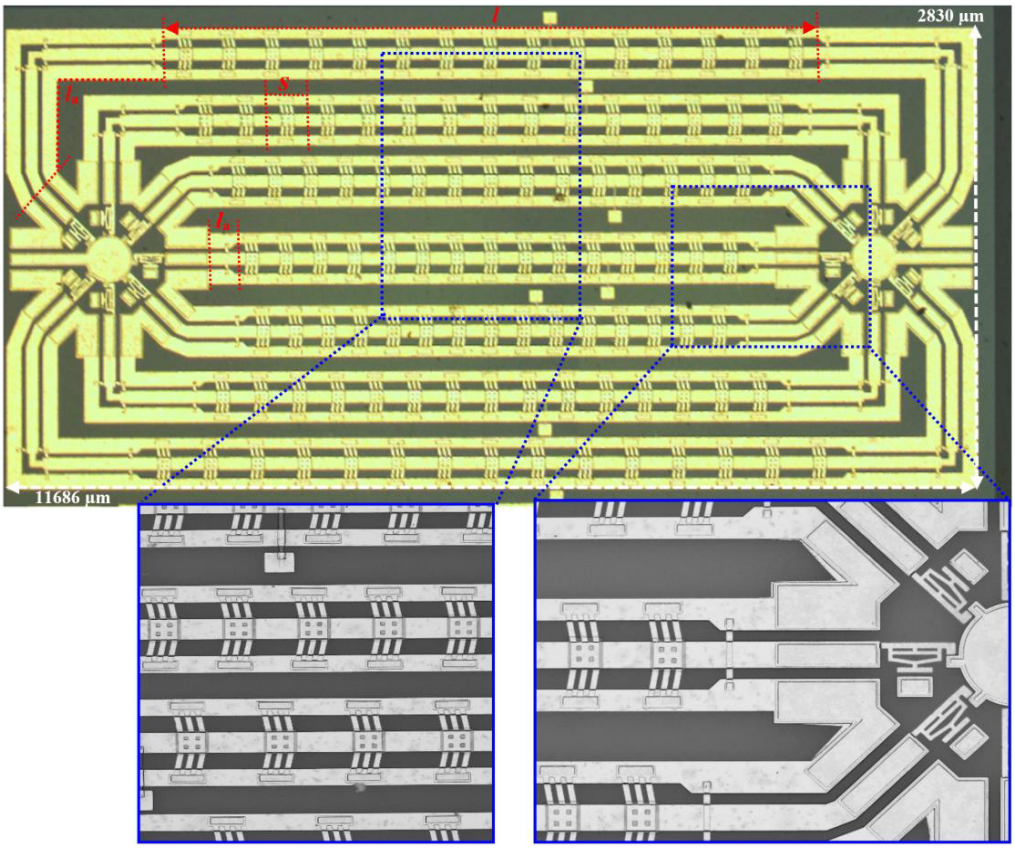

(b)

Figure 5. (a) Detailed design layout and (b) fabricated image of the broadband phase shifter array. Total area of the device is 11.72 mm^2.

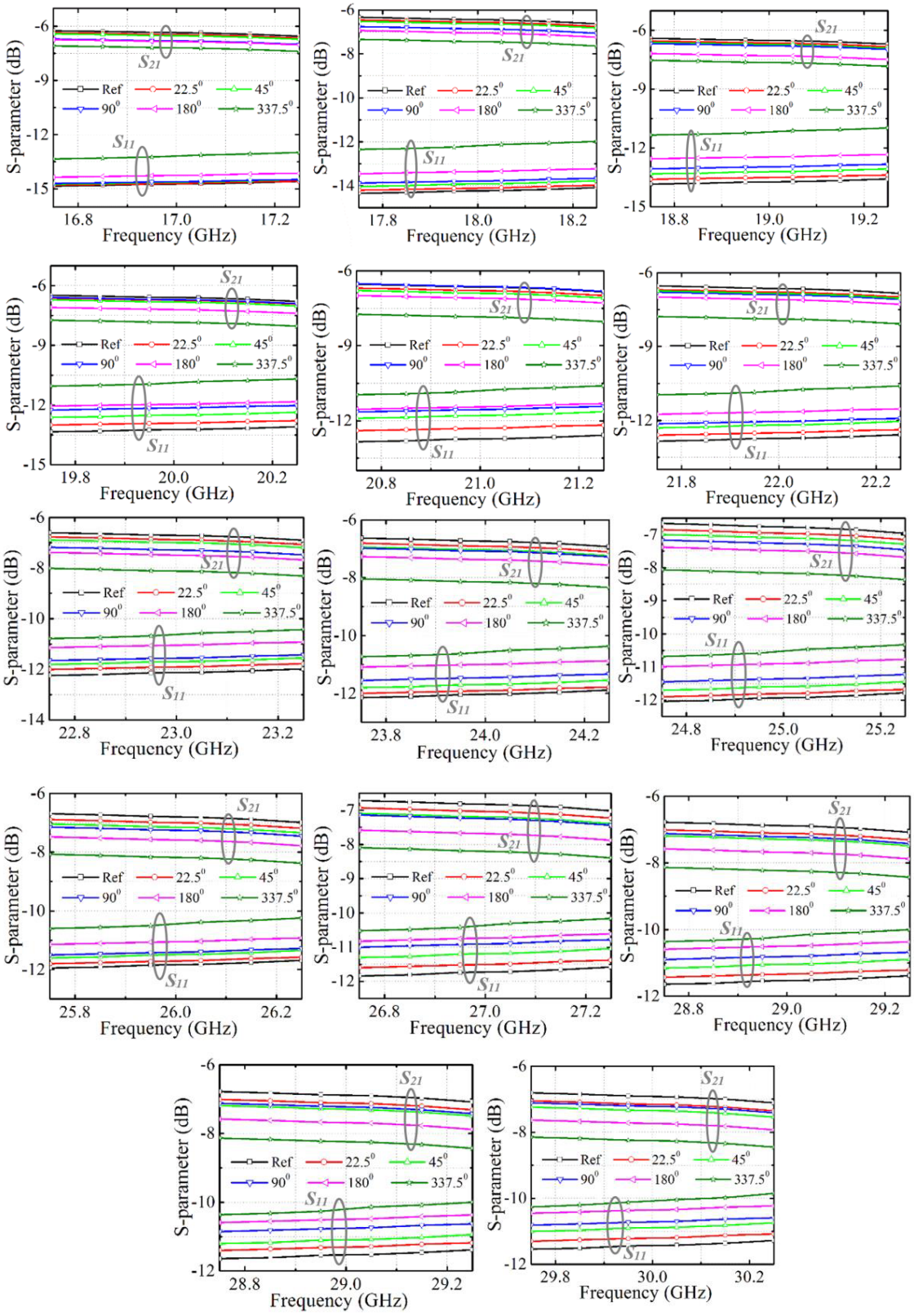

Figure 6. Measured *S*-parameter responses of the broadband phase shifter array over a 500 MHz bandwidth from 17 GHz to 30 GHz. Result shows reponses at six phase states.

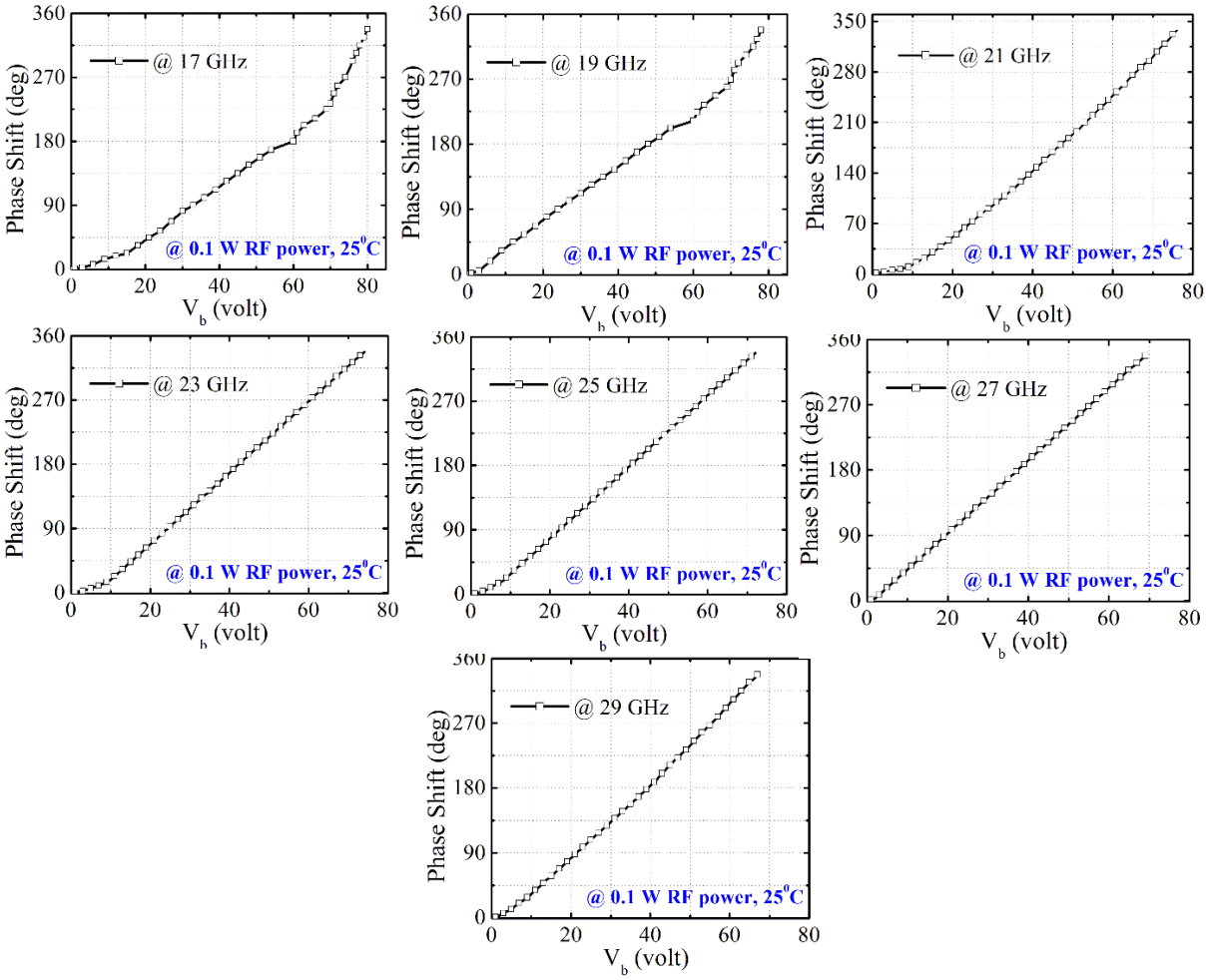

Figure 7. Measured differential phase shift with applied bias voltage of the broadband phase shifter array. Results show performances at every alternative frequencies starting from 17 GHz.

Finally, a complete phase shifter array was designed with seven DMTL structures and two lateral MEMS SP7T switches connected back-to-back. The complete schematic and fabricated image of the analog phase shifter array are depicted in Figs. 5(a)–(b), respectively. All essential parameters are marked in Fig. 5(a) for better clarity. The total area of the phase shifter array is 11.72 mm^2. To achieve the optimum performance, three high frequency DMTL phase shifter cells (25–26 GHz, 27–28 GHz, and 29–30 GHz) were connected at the middle just to reduce the loss from additional line lengths, as depicted in Fig. 5(b). The proposed broadband analog phase shifter demonstrates measured average matching of $>$ 10 dB and loss of $<$ 6.94 dB, as shown in Fig. 6. Each frequency point was checked over a 500 MHz bandwidth, and corresponding changes in matching and loss were recorded. Finally, differential phase shift was measured with applied voltages (V_b) at fourteen frequency points between 17 and 30 GHz. Fig. 7 shows phase shift versus applied voltage at every alternative frequency starting from 17 GHz. All these measurements were carried out at 0.1 W of RF power at 25°C. The average phase error of 1° was obtained from the measurements up to 30 GHz with same applied voltages between 66 and 80 V. The overall phase shift variations are from 0 to 337.5° at each frequency and average phase error of 1° up to 30 GHz. It is indicated that the proposed analog phase shifter can operate as a 4-bit phase shifter. Note that a little variation of this phase error was mostly due to the nonuniform beam thickness (3.43–3.56 µm) during electroplating process. Nonuniform distributions of C_{lu} and C_{ld} happened throughout the actuation process under the same bias voltage. These results provide a clear data set for readers to obtain required amount of phase shift by fine tuning of the MEMS bridges.

Table 1. Complete performance list of the proposed wide-band phase shifter array.

Frequency (GHz)	Avg. S_{11} (dB)	Avg. S_{21} (dB)	Avg. $\Delta\phi_E$ (deg)	Voltage (V)	PS No:
17 GHz	> 14.6	6.4	1.03°	80.2	PS-1
18 GHz	> 14	6.47	1°	78.6	PS-1
19 GHz	> 13.8	6.67	0.97°	77.4	PS-2
20 GHz	> 13.6	6.683	0.95°	76.6	PS-2
21 GHz	> 13.18	6.8	0.93°	75.3	PS-3
22 GHz	> 12.96	6.815	0.88°	~ 74	PS-3
23 GHz	> 12.85	6.92	0.74°	72.5	PS-4
24 GHz	> 12.44	6.97	0.67°	71.2	PS-4
25 GHz	> 12.31	7.1	0.57°	70.4	PS-5
26 GHz	> 12.14	7.18	0.41°	~ 69	PS-5
27 GHz	> 12.04	7.24	0.33°	69.8	PS-6
28 GHz	> 11.8	7.247	0.22°	68.4	PS-6
29 GHz	> 11.32	7.38	0.12°	67.5	PS-7
30 GHz	> 10.89	7.45	0.07°	~ 66	PS-7

Nevertheless, Table 1 provides a complete performance list of the proposed wide-band phase shifter at different operating frequencies. Authors strongly believe that analog tuning of the phase shifter provides better flexibility than its digital counterpart. In a nutshell, the proposed wideband phase shifter can demonstrate any phase shift at any frequencies between 17 and 30 GHz without compromising the S-parameter performances. However, flexibility is more at higher frequencies (> 24 GHz) than lower frequencies over the range. Actuation voltage limits working range because lower frequency demands more capacitances with more bias voltage. Finally, Table 2 shows detailed performance comparison of the proposed wideband phase shifter with the current state-of-the-art MMIC, CMOS, and MEMS phase shifters.

5. RELIABILITY MEASUREMENTS: PHASE IV

One of the biggest challenges of the MEMS based devices is the reliability. To ensure optimum performances from the wideband phase shifter, an extensive reliability testing process was adopted with 0.1–1 W RF power up to 1 billion (B) cycles. Reliability test setup and related descriptions are given in [27]. Initially, the reliability of individual controlling elements was checked, including single lateral MEMS switch, SP7T switch, and MEMS bridge. Finally, the complete device performances were tested up to 1B cycles.

5.1. Reliability Testing of the Controlling Elements

Reliability and power handling measurements were performed on all the controlling elements with 0.1–1 W of RF powers. Initially, variation of single switch contact resistance (R_c) was measured using a four-point probe method with applied bias and reported in Fig. 3(a). The similar measurement was also repeated on the SP7T MEMS switch, and related variations of average R_c from all switches were recorded and plotted in Fig. 3(a). Next, single lateral switch power handling capability was measured periodically at 20 kHz switching rate with 0.1–1 W of power at 2 GHz, as shown in Fig. 8(a). The test was performed up to 1B cycles, and it performed satisfactorily without contact degradation between cantilever beam and output transmission line. Note that the proposed switch is dielectric less, and charging problems were completely avoided. A square waveform was applied to the switch with 50 µsec period (ramp of 15 µsec rise time and 10 µsec fall time).

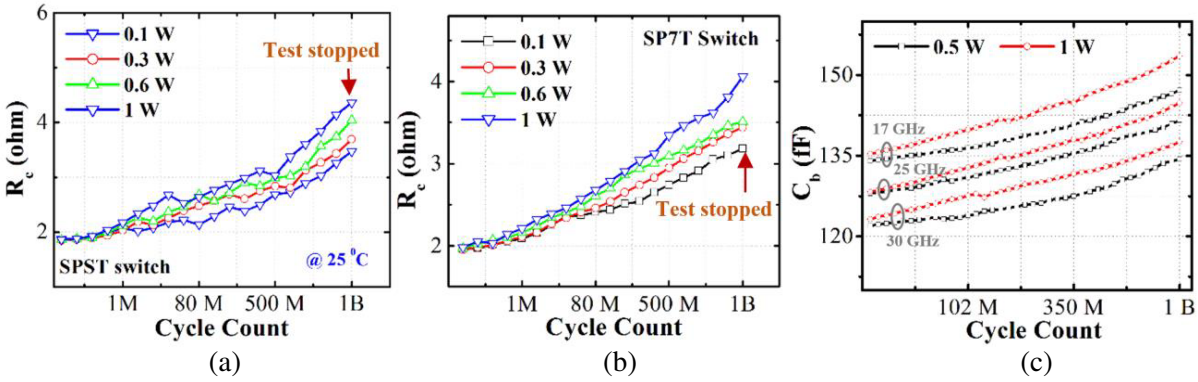

Figure 8. Reliability responses of all individual controlling elements where (a), (b) variation of R_C as a function of cycle count from 0.1–1 W of RF power for single switch (SPST) and SP7T switch, respectively and (c) bridge capacitance (C_b) variations with 0.5–1 W of RF power up to 1B cycles.

Table 2. State-of-the-art performance comparisons of the proposed broadband phase shifter with other reported designs using MMIC, CMOS and MEMS phase shifters.

Comparison with other Reported Broadband MMIC and CMOS Phase Shifters							
Ref, Year	**Frequency (GHz)**	**Phase Shift (°)**	**Resolution (°)**	**Avg. IL (dB)**	**Avg. RL (dB)**	**Avg. Phase Error (°)**	
[7], 2006	12	0–360	11.25	-14.5 ± 0.5	< -10	12	
[8], 2007	15–26	0–360	22.5	-3.8	< -10	9.7	
[9], 2008	35 (31–38)	0–360	22.5	-13	< -10	11	
[10], 2010	6–18	0–360	11.25	N/A	< -10	5.6	
[11], 2013	10 (5–20)	0–360	11.25	-27	< -12	N/A	
This Work (Analog type)	**17–30**	**0–360**	**Any**	**−6.94**	**< 10**	**∼ 1°**	
Comparison with other Reported Broadband MEMS Phase Shifters							
Ref, Year	**Frequency (GHz)**	**Phase Shift (°)**	**Resolution (°)**	**Avg. IL (dB)**	**Avg. RL (dB)**	**Avg. Phase Error (°)**	**Size (mm^2)**
[6], 2003	15–45	0–40	10	-3.5	< -10	4.9	NA
[20], 2003	10	0–360	22.5	-1.25 ± 0.5	< 14	2.3	21.3
[12], 2008	18	0–360	5.625	-2.8	< 7	N/A	40
[13], 2008	10	0–360	11.25	-4.5	< 10	10	9.23
[21], 2011	60	0–360	90°	-2.5	< 12	1	4
[14], 2012	15	0–360	22.5	-1.7	< 10	7	N/A
[15], 2013	15–40	0–180	10	-3.6	< 19	1.3	63.72
[16], 2013	17.25	0–360	11.25	-5.4	< 14	1.35	36
[17], 2014	10	0–360	11.25	-4.72	< 12	3.65	19.4
[18], 2015	12–25	0–360	11.25	-4.4	< 14	6	15.6
[19], 2015	17	0–360	11.25	-2.65	< 22	0.68	13
This Work (Analog type)	**17–30**	**0–360**	**Any**	**−6.94**	**< 10**	**∼ 1°**	**∼ 11.72**

The amplitude of the DC waveform was set to +95 V, and 25 μsec time span was maintained during the contacting period for efficient signal transmission. Bias-Tee and cable losses were normalized and not accounted during the testing stages. R_c was recorded periodically, and switch can withstand up to 1B cycles at 0.1–1 W power. The R_c variations of 1.88–4.3 Ω were noticed during experiment. Finally, power handling capability of the SP7T switch was measured with the same setup and under same operating condition. The average R_c variation from the SP7T switch is plotted in Fig. 8(b). Note that reliability testing was limited up to 1 W for the SP7T switch since each arm was actuated independently. Changes in R_c were mostly due to contact contaminants with excessive temperature rise on contact at higher RF power in the non-hermetic conditions.

Furthermore, reliability of the MEMS bridge was checked with 0.5–1 W of power and with three bias voltages (66 V, 73 V and 80 V). The related changes in C_b were recorded and plotted in Fig. 8(c). The maximum change of ∼ 16 fF (135–151 fF) was found with 80 V bias voltage at 17 GHz. Note that this measurement was carried out at 17 GHz, 25 GHz, and 30 GHz. The C_b variation was mostly due to reduction of beam restoring force over the continuous actuation process. Note that no adverse effect of dielectric changing was noticed during measurement.

5.2. Reliability Testing of the Wideband Phase Shifter Array

Reliability of the complete wideband phase shifter array was extensively tested at every alternative frequency from seven DMTL cells starting from 18 GHz. Each arm was activated by tuning two lateral MEMS switch, and then MEMS bridges were actuated accordingly over the cycle. The same V_b values were applied, and related changes in device losses were recorded up to 1B cycles with 0.5–1 W of RF

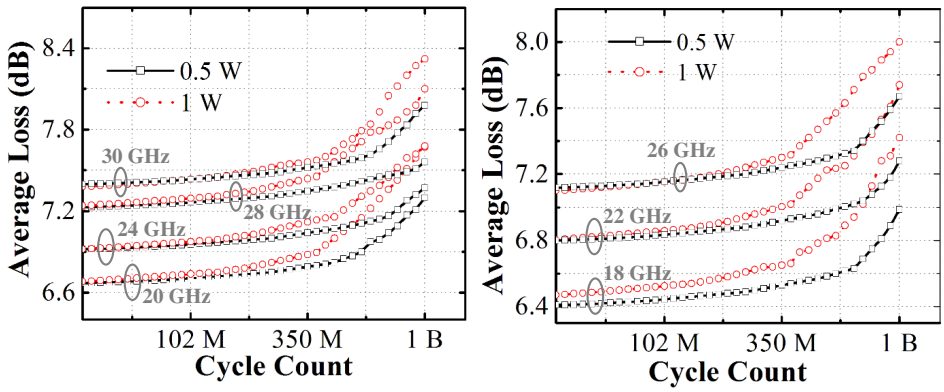

Figure 9. Reliability results of the wide-band analog phase shifter array at seven even frequencies over 17–30 GHz.

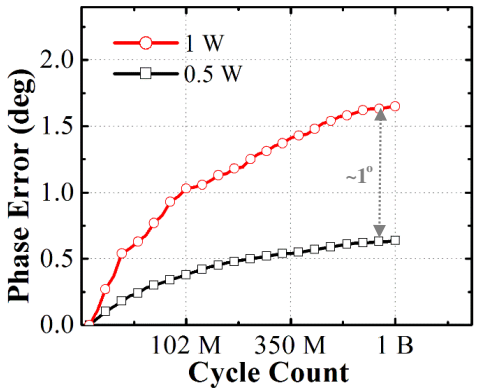

Figure 10. Reliability responses of the average phase error variations up to 1B cycles with 0.5–1 of RF power from the wide-band phase shifter array.

power. Average insertion loss values are plotted in Fig. 9 at seven frequencies with 0.5 and 1 W of RF power up to 1B cycles. Results show that phase shifter works satisfactorily up to 1B cycles with maximum average loss variation of 7.35–8.3 dB from 0.5 to 1 W of power. All related frequencies are marked in Fig. 9 for better clarity. Nevertheless, phase errors were also noted during the measurements, and average phase errors from the wideband phase shifter array were recorded systematically and plotted in Fig. 10 against 0.5 W and 1 W of RF power up to 1B cycles. The maximum change in average phase error was $\sim 1^\circ$ from the device from 0.5 W and 1 W of RF power levels. Reliability operation was mostly dominated by the electro-migration of current density [29–31]. Note that MEMS bridges are always actuated over the point of stability in a DMTL, and it leads to higher reliability. A shunt protection technique can also be used in the structure [32]. Note that device was tested up to 1B cycles (with 1 W power) in a standard lab environment.

6. CONCLUSION

In this work, design, development, and extensive characterization of a wide-band analog MEMS phase shifter array is presented using two SP7T switches and seven DMTL structures. Behaviours of all individual functional blocks (single lateral switch, SP7T switches, and DMTL unit cell) were carefully considered to ensure the optimum device performances over the frequency range of interest. Reliability of all controlling elements has been extensively tested up to 1B cycles and presented systematically. The complete phase shifter demonstrates the measured average insertion of 6.94 dB, average return loss of 10 dB, and maximum average phase error of $\sim 1^\circ$ up to 30 GHz. The proposed phase shift array is operational up to 1 billion cycles with 1 W of incident RF power.

In addition, phase shifter performance variation over the cycle was explicitly shown. Complete area of the proposed wide-band phase shifter array is 11.72 mm^2, and it is also comparable with other reported MEMS based phase shifters. Performances of the proposed device are compared with other state-of-the-art technologies like MMIC and CMOS. In the opinion of authors, this is the first reported wideband analog MEMS phase shifter array in the literature that has flexible resolution where any phase shift can be obtained over 17–30 GHz frequency based on specific DC bias. The performance could be improved further with a hermetic condition, and authors intend to do zero-level packaging on the reported device in future.

REFERENCES

1. Lucyszyn, S., *Advanced RF MEMS*, Cambridge University Press, Aug. 2010.
2. Muller, S., P. Scheele, C. Weil, M. Wittek, C. Hock, and R. Jakoby, "Tunable passive phase shifter for microwave applications using highly anisotropic liquid crystals," *IEEE MTT-S Int. Microw. Symp. Dig.*, 1153–1156, Fort Worth, TX, USA, Jun. 2004.
3. Chang, Q., Q. Li, Z. Zhang, Q. Min, Y. Tong, and Y. Su, "A tunable broadband photonic RF phase shifter based on a silicon microring resonator," *IEEE Photon. Technol. Lett.*, Vol. 21, No. 1, 60–62, Jan. 2003.
4. Erker, G. E., S. A. Nagra, L. Yu, P. Periaswamy, R. T. Taylor, J. Speck, and R. A. York, "Monolithic Ka-band phase shifter using voltage tunable $BaSrTiO_3$ parallel plate capacitors," *IEEE Microw. Guided Wave Lett.*, Vol. 10, No. 1, 10–12, Jan. 2000.
5. Rebeiz, G. M., *RF MEMS Theory, Design, and Technology*, Wiley, Hoboken, NJ, 2003.
6. Lee, S., J.-H. Park, H.-T. Kim, J.-M. Kim, Y.-K. Kim, and Y. Kwon, "Low-loss analog and digital reflection-type MEMS phase shifters with 1 : 3 bandwidth," *IEEE Trans. Microw. Theory Techn.*, Vol. 52, No. 1, 211–219, Jan. 2004.
7. Kang, D.-W., H. D. Lee, C.-H. Kim, and S. Hong, "Ku-band MMIC phase shifter using a parallel resonator with 0.18-µm CMOS technology," *IEEE Trans. Microw. Theory Tech.*, Vol. 54, No. 1, 294–301, Jan. 2006.
8. Koh, K.-J. and G. M. Rebeiz, "0.13-µm CMOS phase shifters for X-, Ku-, and K-band phased arrays," *IEEE J. Solid-State Circuits*, Vol. 42, No. 11, 2535–2546, Nov. 2007.

9. Min, B. and G. M. Rebeiz, "Single-ended and differential-band BiCMOS phased array front-ends," *IEEE J. Solid-State Circuits*, Vol. 43, No. 10, 2239–2250, Oct. 2008.
10. Koh, K.-J. and G. M. Rebeiz, "A 6–18 GHz 5-bit active phase shifter," *IEEE MTT-S Int. Microw. Symp. Dig.*, 792–795, Montreal, Anaheim, CA, May 2010.
11. Choi, J. Y., M.-K. Cho, D. Baek, and J.-G. Kim, "A 5–20 GHz 5-bit true time delay circuit in 0.18 µm CMOS technology," *J. Semiconductor Tech. Science*, Vol. 13, No. 3, 193–197, Jun. 2013.
12. Nordquist, C. D., C. W. Dyck, G. M. Kraus, C. T. Sullivan, F. Austin, P. S. Finnegan, and M. H. Ballance, "Ku-band six-bit RF MEMS time delay network," *Compound Semiconductor Integrated Circuits Symposium, 2008, CSIC'08*, IEEE, Oct. 2008.
13. Morton, M. A. and J. Papapolymerou, "A packaged MEMS-based 5-bit X-band high-pass/low-pass phase shifter," *IEEE Trans. Microw. Theory Techn.*, Vol. 56, No. 9, 2025–2031, Aug. 2008.
14. Pillans, B., L. Coryell, A. Malczewski, C. Moody, F. Morris, and A. Brown, "Advances in RF MEMS phase shifters from 15 GHz to 35 GHz," *IEEE MTT-S Int. Microw. Symp. Dig.*, 1–3, Montreal, QC, Canada, Jun. 2012.
15. Unlu, M., S. Demir, and T. Akin, "A 15–40-GHz frequency reconfigurable RF MEMS phase shifter," *IEEE Trans. Microw. Theory Tech.*, Vol. 61, No. 8, 2397–2402, Aug. 2013.
16. Dey, S. and S. K. Koul, "Design and development of a CPW-based 5-bit switched-line phase shifter using inline metal contact MEMS series switches for 17.25 GHz transmit/receive module application," *J. Micromech. Microeng.*, Vol. 24, No. 1, 24 pages, Nov. 2013.
17. Dey, S. and S. K. Koul, "Design, development and characterization of an X-band 5 bit DMTL phase shifter using an inline MEMS bridge and MAM capacitors," *J. Micromech. Microeng.*, Vol. 24, No. 1, 15 pages, Jun. 2014.
18. Dey, S. and S. K. Koul, "10–25-GHz frequency reconfigurable MEMS 5-bit phase shifter using push-pull actuator based toggle mechanism," *J. Micromech. Microeng.*, Vol. 25, No. 6, 1–20, May 2015.
19. Dey, S. and S. K. Koul, 'Reliability analysis of Ku-band 5-bit phase shifters using MEMS SP4T and SPDT switches," *IEEE Trans. Microw. Theory Tech.*, Vol. 60, No. 9, 2863–2874, 2012.
20. Tan, G.-L., R. Mihailovich, J. Hacker, J. De Natale, and G. M. Rebeiz, "Low-loss 2- and 4-bit TTD MEMS phase shifters based on SP4T switches," *IEEE Trans. Microw. Theory Techn.*, Vol. 51, No. 1, 297–304, Jan. 2003.
21. Gong, S., H. Shen, and N. S. Barker, "A 60-GHz 2-bit switched-line phase shifter using SP4T RF-MEMS switches," *IEEE Trans. Microw. Theory Techn.*, Vol. 59, No. 4, 894–900, Apr. 2011.
22. Baghchehsaraei, Z., A. Vorobyov, J. Åberg, E. Fourn, R. Sauleau, and J. Oberhammer, "Waveguide-integrated MEMS-based phase shifter for phased array antenna," *IET Microw. Antennas Propag.*, Vol. 8, No. 4, 235–243, 2014.
23. San, H. S., X. Y. Chen, P. Xu, G. Li, and L. X. Zhan, "Using metal insulator-semiconductor capacitor to investigate the charge accumulation in capacitive RF MEMS switches," *Appl. Phys. Lett.*, Vol. 93, No. 6, 063506-1–063506-3, Aug. 2008.
24. Dey, S. and S. K. Koul, "Broadband, reliable and compact lateral MEMS SP4T and SP7T switching networks for 5G applications," *IEEE MTTS International Microwave and RF Conference*, Bombay, India, Dec. 13–15, 2019.
25. Dey, S., S. K. Koul, A. Poddar, and U. Rodhe, "Reliable and compact 3-bit and 4-bit phase shifters using MEMS SP4T and SP8T switches," *IEEE J. Microelectromech. Syst.*, Vol. 27, No. 1, 113–124, Feb. 2018.
26. Dey, S., S. K. Koul, A. K. Poddar, and U. L. Rodhe, "Compact, broadband and reliable lateral MEMS switching networks for 5G communications," *Progress In Electromagnetic Research M*, Vol. 86, 163–171, 2019.
27. Koul, S. K. and S. Dey, "MEMS K-band 4-bit phase shifter using two back to back SP16T switching networks," *IEEE J. Microelectromech. Syst.*, Vol. 27, No. 4, 643–655, Feb. 2018.
28. Mahameed, R. and G. M. Rebeiz, "A high-power temperature stable electrostatic RF MEMS capacitive switch based on thermal buckle-beam design," *IEEE J. Microelectromech. Syst.*, Vol. 19, No. 4, 816–826, Aug. 2010.

29. Dey, S. and S. K. Koul, "Reliable, compact, and tunable MEMS bandpass filter using arrays of series and shunt bridges for 28-GHz 5G applications," *IEEE Trans. Microw. Theory Tech.*, Vol. 69, No. 1, 75–88, Jan. 2021.
30. Dey, S., S. K. Koul, A. K. Poddar, and U. L. Rohde, "Extensive performance evaluations of RFMEMS single-pole-multi-throw (SP3T to SP14T) switches up to X-band frequency," *J. Micromech. Microeng.*, Vol. 27, No. 1, 10 pages, Nov. 2016.
31. Koul, S. K., S. Dey, A. K. Poddar, and U. L. Rohde, "Ka-band reliable and compact 3-bit true-time-delay phase shifter using MEMS single-pole-eight-throw switching networks," *J. Micromech. Microeng.*, Vol. 26, No. 10, 9 pages, Aug. 2016.
32. Liu, Y., Y. Bey, and X. Liu, "High-power high-isolation RF-MEMS switches with enhanced hot-switching reliability using a shunt protection technique," *IEEE Trans. Microw. Theory Tech.*, Vol. 65, No. 9, 3188–3199, Mar. 2017.